THE JOURNAL OF PHYSICAL CHEMISTRY A

ARTICLE

pubs.acs.org/JPCA

Characterizing the Rovibrational Distribution of CD_2CD_2OH Radicals Produced via the Photodissociation of 2-Bromoethanol-d_4

Caroline C. Womack,[†] Ryan S. Booth,[†] Matthew D. Brynteson,[†] Laurie J. Butler,[*,†] and David E. Szpunar[*,‡]

[†]Department of Chemistry and the James Franck Institute, University of Chicago, Chicago Illinois 60637, United States

[‡]Department of Biological, Chemical, and Physical Sciences, Roosevelt University, Schaumburg, Illinois 60173, United States

Supporting Information

ABSTRACT: This work characterizes the internal energy distribution of the CD_2CD_2OH radical formed via photodissociation of 2-bromoethanol-d_4. The CD_2CD_2OH radical is the first radical adduct in the addition of the hydroxyl radical to C_2D_4 and the product branching of the OH + C_2D_4 reaction is dependent on the total internal energy of this adduct and how that energy is partitioned between rotation and vibration. Using a combination of a velocity map imaging apparatus and a crossed laser-molecular beam scattering apparatus, we photodissociate the $BrCD_2CD_2OH$ precursor at 193 nm and measure the velocity distributions of the Br atoms, resolving the $Br(^2P_{1/2})$ and $Br(^2P_{3/2})$ states with [2 + 1] resonance enhanced multiphoton ionization (REMPI) on the imaging apparatus. We also detect the velocity distribution of the subset of the nascent momentum-matched CD_2CD_2OH cofragments that are formed stable to subsequent dissociation. Invoking conservation of momentum and conservation of energy and a recently developed impulsive model, we determine the vibrational energy distribution of the nascent CD_2CD_2OH radicals from the measured velocity distributions.

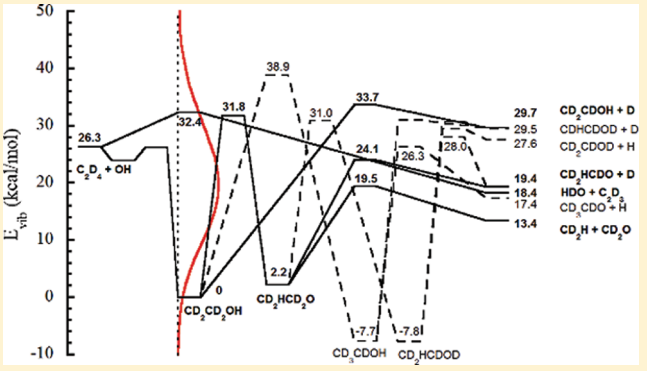

I. INTRODUCTION

The reaction of hydroxyl radicals with ethene has been the focus of a number of experimental[1−21] and theoretical[22−28] studies in the past few decades. This interest is strong due to the role that OH + alkene reactions play in atmospheric and combustion chemistry. At high temperatures, the dominant mechanism of the OH + ethene reaction is the abstraction of a hydrogen atom to form H_2O + CH_2CH. However, at low temperatures, the overall reaction rate is driven by an alternate mechanism in which the hydroxyl radical electrophilically adds to one of the carbons to form the long-lived CH_2CH_2OH radical intermediate. This adduct is collisionally stabilized at high pressures, but with sufficient energy it may undergo dissociation, either back to OH + ethene or to other products. The overall product branching in this reaction is key to the construction of accurate combustion models. The OH-initiated oxidation of alkenes has been suggested to be one of the first steps toward the formation of secondary organic aerosols.[29]

The overall rate of the OH + ethene reaction has been studied extensively via a number of experimental techniques at temperatures ranging from 96 K[1] to 1300 K,[2] though the majority of studies were conducted near room temperature. The initial addition proceeds through a van der Waals complex, $[C_2H_4]\cdots OH$,[22,23] and exhibits a negative activation energy. Tully and co-workers determined the overall high-pressure temperature-dependent rate constant by monitoring [OH] via laser fluorescence following exposure to C_2H_4 at a wide range of temperatures and pressures.[3,4] They noted that, at temperatures near 500 K, the [OH] signal exhibited a nonexponential decay and attributed it to internally excited CH_2CH_2OH radicals dissociating. They concluded that virtually all of the CH_2CH_2OH radicals with sufficient energy to decompose would dissociate back to OH + C_2H_4, rather than form other products. An early mass spectrometric study[5] noted the presence of products with m/e = 44 following the reaction of OH with ethene. This product was attributed to acetaldehyde formed by the dissociation of CH_2CH_2OH adducts. Ethenol, CH_2CHOH, was largely ignored as a possible product in combustion models, as acetaldehyde is the more thermodynamically stable isomer. However, Cool and co-workers recently discovered both ethenol and acetaldehyde products in flames of ethene, underscoring the need to examine the product channels more closely, the ethenol channel in particular.[6−8]

Sosa et al. calculated the stationary points on the potential energy surface (PES) of the OH + ethene reaction at the HF/6-31G* level of theory.[24] Two more radical intermediates formed by isomerization of the initial CH_2CH_2OH adduct were characterized,

Received: June 24, 2011
Revised: September 21, 2011
Published: November 09, 2011

as well as several product channels. In addition to the ethenol + H and acetaldehyde + H product channels, they included the $CH_3 + CH_2O$ channel following isomerization of the CH_2CH_2OH radicals to the ethoxy radical, CH_3CH_2O. Subsequent theoretical studies at the UQCISD[23,26] and UB3LYP[23] levels of theory confirmed these pathways and added two additional pathways leading to ethenol + H; one direct dissociation pathway of the CH_2CH_2OH radical and one pathway following the isomerization of CH_2CH_2OH to CH_3CHOH. Senosiain et al.[23] used statistical transition state theories to predict the branching fractions to the direct abstraction products and the product formed following the addition/elimination mechanism, as a function of T and P. They predicted that, of the products resulting from an addition mechanism, the formaldehyde + methyl channel should dominate at low temperatures at the collisionless limit (e.g., no collisional stabilization of the radical intermediate), with the ethenol + H channel growing in importance as the temperature increased.

Several groups have photodissociated 2-haloethanols to yield CH_2CH_2OH radicals in conjunction with a halogen atom.[30−34] Hintsa et al. photodissociated 2-bromoethanol at 193 nm and measured the kinetic energy imparted to the fragments using photofragment translational spectroscopy.[31] They observed the dissociation of some of the CH_2CH_2OH radicals to OH + ethene and measured the velocity distribution of the portion of the CH_2CH_2OH radicals formed stable to this dissociation. Noting that these stable radicals had total internal energy up to 43 kcal/mol, well above the barrier to dissociate to OH + ethene, they concluded that the photodissociation partitioned a large amount of energy into the rotational degrees of freedom of the CH_2CH_2OH radicals, resulting in their metastability.[31] They also noted that over a 12 kcal/mol range in translational energies, some of the radicals were formed stable and others dissociated and suggested that this might be due to a portion of the radicals being formed in conjunction with spin−orbit excited Br atoms. The electron bombardment detection method did not allow them to separately resolve the velocity distributions of the $Br(^2P_{1/2})$ and $Br(^2P_{3/2})$ cofragments, which prohibited them from pursuing a quantitative analysis of the distribution of stable radicals. Sapers and Hess subsequently photodissociated $BrCH_2CH_2OH$ at 202 nm and monitored the production of OH radicals.[30] The linear increase in OH signal upon increasing laser power confirmed that OH radicals formed as a result of a secondary dissociation of internally excited CH_2CH_2OH radicals, not as a result of the absorption of a second photon, in agreement with Hintsa et al.'s assignment of their spectrum at $m/e = 17$.[31]

In our previous work, we studied the product branching of the internally excited CH_2CH_2OH radicals generated by the dissociation of the photolytic precursor 2-bromoethanol.[35] Among the product channels detected in the dissociation of the vibrationally excited radicals were $H_2O + C_2H_3$ and $CH_3 + CH_2O$ and fragments detected with a mass-to-charge ratio of 44, attributed largely to the ethenol + H pathway. In an effort to better characterize these product channels, we have begun a comprehensive study of the $OH + C_2D_4$ reaction, beginning with the first radical adduct CD_2CD_2OH, to elucidate the various products based on their mass, photoionization spectra, and velocity distributions. We generate this radical in a range of internal energies by dissociating the parent molecule 2-bromoethanol-1,1,2,2-d_4, $BrCD_2CD_2OH$, at 193 nm, and then probe the nascent stable radicals with either VUV photoionization or 200 eV electron bombardment ionization. Reisler and co-workers[33] recently studied the product pathways of the CD_2CD_2OH radical, in particular, the pathways leading to D products. They used $[1 + 1']$ resonance enhanced multiphoton ionization (REMPI) to detect deuterium, which is formed in conjunction with ethenol or with acetaldehyde. While they were unable to experimentally distinguish between the $CD_2CDOH + D$ and $CD_2HCDO + D$ pathways, they were able to confirm the presence of at least one D-loss channel that is the result of secondary dissociation of vibrationally excited CD_2CD_2OH radicals. Their RRKM calculations suggested that at all energies, the acetaldehyde channel should be a minor contributor compared to the ethenol channel.

To accurately compare these product branching studies on the partially deuterated system to theoretical predictions, it is important to characterize the vibrational energy distribution of the nascent CD_2CD_2OH radicals. This paper reports the determination of that nascent vibrational energy distribution. We determine the total internal energy distribution by measuring the spin−orbit state selected velocity distributions of the bromine cofragment, then use a recently introduced model[32] to model the partitioning of the total internal energy to rotation and vibration. We test the model by comparing its prediction to our measured velocity distribution of stable CD_2CD_2OH radicals. We find the model accurately predicts that distribution with no adjustable parameters.

II. EXPERIMENTAL DETAILS

We use two methods to characterize the distribution of translational energies imparted to the Br and CD_2CD_2OH radical fragments following the dissociation of 2-bromoethanol-d_4; a velocity map imaging apparatus, using $[2 + 1]$ REMPI and VUV photoionization detection and a crossed laser-molecular beam scattering apparatus in conjunction with 200 eV electron bombardment ionization. In both apparatuses, we photodissociate the precursor, measure velocity distributions of the two fragments under collision-free conditions, and invoke conservation of momentum to determine a center-of-mass translational energy distribution, $P(E_T)$, of the dissociation events. The primary dissociation of 2-bromoethanol-d_4 leaves the CD_2CD_2OH radical fragments with a range of internal energies spanning the energetic barriers to secondary dissociation. Thus, the velocity distribution obtained by detecting the Br atoms allows us to derive a $P(E_T)$ of all dissociation events. The velocity distribution obtained by detecting the CD_2CD_2OH radicals determines the portion of the $P(E_T)$ of the dissociation events that resulted in radicals with low enough vibrational energy to be detected as stable radicals on the time scale of the measurement. The neutral radicals are ionized 40 ns after the photodissociation in the imaging apparatus, and at least 100 μs after the photodissociation in the crossed laser-molecular beam apparatus.

The crossed laser-molecular beam has been a widely used method for detecting time-of-flight spectra of photoproducts. The benefit of its detection scheme, 200 eV electron bombardment, is that essentially any product formed may be detected. The major drawback of this "universal" detector is that many products undergo dissociative ionization to form smaller ions instead of parent ions, often making identification of the neutral product difficult. The velocity map imaging apparatus, on the other hand, utilizes a "soft" photoionization detection scheme, largely eliminating the problem of dissociative ionization and thus confirming the identity of certain products. Additionally, the velocity map imaging apparatus utilizes $[2 + 1]$ REMPI, allowing

for the state-selective detection of bromine. For these reasons, it is beneficial to complement the time-of-flight spectra of the fragments obtained on the crossed laser-molecular beam apparatus with the velocity distributions of the fragments obtained on the velocity map imaging apparatus.

A. Velocity Map Imaging Apparatus. The velocity map imaging apparatus, modeled on the design of Eppink and Parker[36,37] has been described in detail elsewhere.[32] In short, a 1.2% molecular beam of 2-bromoethanol-1,1,2,2-d_4 (Sigma-Aldrich, 98% D atoms, used without further purification) was generated by seeding the vapor pressure of the liquid sample (heated to 40 °C) in helium to a total backing pressure of 500 Torr. The gaseous mixture was supersonically expanded through a General Valve Iota One pulsed valve operating at 20 Hz, mounted in a vacuum chamber maintained at 10^{-7} Torr. The nozzle was heated to 80 °C to minimize the formation of molecular clusters in the beam. A supersonic expansion in a light seed gas such as helium typically results in the cooling of the relative translational and rotational degrees of freedom but only minimal cooling of the vibrational degrees of freedom of the molecule.[38,39] After passing through a skimmer, the beam of $BrCD_2CD_2OH$ molecules intersected the vertically polarized 193.3 nm output of a pulsed GAM EX10 excimer laser. The photon excites the 2-bromoethanol-d_4 molecule to a repulsive excited state, cleaving the C−Br bond. The rectangular cross section of the laser beam initially measured 8 by 4 mm, and was focused into the vacuum chamber by a UV fused silica focusing lens to a point approximately 3 cm before the interaction region with the molecular beam. The photolysis laser and the photoionization laser propagated perpendicularly to the molecular beam, and antiparallel to each other. The photolysis laser pulses typically had energies below 1 mJ/pulse. The recoiling Br and CD_2CD_2OH radical fragments were photoionized approximately 40 ns later, and the spherically expanding cloud of ions was accelerated down the grounded time-of-flight tube by an electrostatic lens assembly. This assembly consisted of a repeller plate and an extractor plate maintained at a voltage ratio of 1.4:1. All radicals created with the same velocity vector were mapped to nearly the same point on the detector, regardless of initial position.

The Br atoms were ionized via [2 + 1] REMPI, using the frequency-tripled output of a Lambda-Physik dye laser pumped by the second harmonic of a Nd:YAG Continuum Powerlite laser. The ground ($^2P_{3/2}$) and excited ($^2P_{1/2}$) spin−orbit state Br atoms were state-selectively ionized by three 233.681 nm photons ($5p\ ^4P_{1/2} \leftarrow 4p\ ^2P_{3/2}$) and three 234.021 photons ($5p\ ^2S_{1/2} \leftarrow 4p\ ^2P_{1/2}$), respectively. Complete signal was obtained by scanning over the Doppler profile 0.008 nm from center in both directions. The CD_2CD_2OH radicals were ionized by the 118 nm light generated by tripling the 355 nm output of an Nd:YAG Continuum Surelite I-20 laser in a xenon cell maintained at 25 Torr. A MgF_2 lens (focal length = 80 mm at λ = 118 nm) separated the xenon cell from the vacuum chamber and focused the 118 nm light.

The detector consisted of a position-sensitive Chevron microchannel plate (MCP) coupled to a P20 phosphor screen. A −750 V gate was applied to the front of the MCP, timed to coincide with the arrival of the fragments with the desired mass. The arrival of the positive ions at the front plate of the MCP triggered an electron cascade and a cooled CCD camera (LaVision Imager 3) recorded the images as they appeared on the phosphor screen, which was maintained at 3.3 kV above the potential of the rear of the MCP. The images were accumulated, summed, and processed using the DaVis software program and Houston's ion-counting method.[40] The sphere of ions is pancaked into a flat disk as it travels down the time-of-flight tube, in the same direction as the initial molecular beam, but the resulting two-dimensional projection of the sphere possesses cylindrical symmetry about the axis defined by the direction of the laser polarization.[41,42] Thus, the velocity distribution and angular distribution of the fragments can be obtained by extracting the three-dimensional distribution using an inverse Abel transform and integrating over all solid angles.[43] The BASEX[44] computer program was used to do these calculations. Invoking conservation of momentum between the two fragments, and correcting for the appropriate Jacobian factor yields the center-of-mass recoil translational energy distribution, $P(E_T)$, of the C−Br fission events.

B. Scattering Apparatus. The crossed laser-molecular beam apparatus has been described in detail elsewhere[45−47] so only a brief description will be provided here. A 1.7% molecular beam was generated by seeding the vapor pressure of the liquid 2-bromoethanol-d_4 sample (heated to 40 °C) in helium to a total backing pressure of 350 Torr. The gaseous mixture was expanded through a pulsed nozzle mounted in a rotating-source chamber maintained at 10^{-5} Torr. The nozzle operated at 100 Hz and was heated to 96 °C to minimize clusters in the beam. The molecular beam passed through two skimmers and intersected the 193 nm output of an unpolarized Lumonics PM-848 excimer laser in the main chamber of the apparatus, maintained at 10^{-6} Torr, cleaving the C−Br bond. The source chamber rotates to allow collection of data at a range of angles. The laser beam propagated in a direction perpendicular to the plane defined by the rotating molecular beam and the fixed detector axis. The laser beam was focused to a cross-sectional area measuring 6 mm^2 in the interaction region. The laser pulses typically had energies of 13−15 mJ/pulse to minimize multiphoton absorptions.

The C−Br bond photofission imparts a distribution of velocities in the center-of-mass reference frame to the Br and CD_2CD_2OH photofragments. The net velocity of the detected fragments is the vector sum of the initial velocity of the parent molecule and the recoil velocity imparted to the fragment upon the dissociation of the C−Br bond. The initial velocity distribution of the 2-bromoethanol-d_4 molecules in the beam was characterized by measuring beam time-of-flight (TOF) spectra at a source angle of 0° as the molecular beam passed through a chopper wheel spinning at 300 Hz. These beam TOF spectra were taken twice a day, as the beam velocity changes as a function of experimental conditions. The number density speed distribution of the molecular beam peaked at 1.19×10^5 cm/s with a full-width at half-maximum (FWHM) of 11.0% when the m/e = 79 TOF spectrum was taken and peaked at 1.59×10^5 cm/s with a FWHM of 6.0% when the m/e = 33 TOF spectrum was taken.

Those neutral fragments that scattered with a net velocity vector pointing into the 1.5° acceptance angle of the differentially pumped detector entered the ionizer, where they were ionized by 200 eV electron bombardment ionization. The ions were accelerated and focused by high-voltage plates and were mass-selected by a quadrupole mass spectrometer and detected by a Daly detector. The signal, which is proportional to the number of ions detected, was counted by a multichannel scaler and recorded as a function of arrival time after the laser fires. The data were accumulated in 2 μs channel bins. The arrival time is the sum of two flight times: the flight time of the neutral fragments from the interaction region with the laser beam to their arrival at the ionizer, and the flight time of the ions through the quadrupole

Table 1. Single-Point Energies, Relative Populations, and Bond Dissociation Energies of the Five Stable Conformers of 2-Bromoethanol-d_4[a]

conformer	energy (0 K; kcal/mol)	energy (353.15 K; kcal/mol)	relative population (%; 353.15 K)	bond dissociation energy (kcal/mol)
Tt	1.25	6.08	7.4	70.71
Tg	1.31	6.02	15.2	70.65
Gt	2.01	6.80	7.2	69.95
Gg	0	4.59	65.4	71.96
Gg′	2.50	7.21	4.8	69.46

[a] The single-point energies are calculated at the G4//B3LYP/6-311++G(3df,2p) level of theory at 0 and 353.15 K, and reported relative to the energy of the lowest energy conformer, Gg, at 0 K. The bond dissociation is obtained by subtracting the sum of the G4 energy of the CD_2CD_2OH radical and $Br(^2P_{3/2})$ from the G4 energy of each conformer.

region. The flight time of the neutral fragments depends on the magnitude and direction of the recoil velocity imparted during the dissociation. The flight time of the ions is proportional to the square root of the mass-to-charge ratio of the ionized fragments. The distribution of center-of-mass recoil translational energies imparted during the dissociation is obtained by a forward convolution fit to the TOF spectrum of the Br fragments. The mass-to-charge ratio of the ionized fragment, the angle at which each spectrum was taken, and the total number of accumulated laser shots are all denoted in the top right-hand corner of each plot.

A time-of-flight spectrum was taken at $m/e = 79$ (Br^+) but no signal was detected above the baseline at $m/e = 49$ ($CD_2CD_2OH^+$) after 1.5×10^6 laser shots. Signal at $m/e = 33$ (CD_2OH^+), however, represents those stable CD_2CD_2OH radicals that have a net velocity vector pointing into the acceptance angle of the detector but dissociatively ionize to CD_2OH^+ when bombarded with 200 eV electrons. Thus, it yields the same recoil translational energy distribution as the $m/e = 49$ spectrum would, once the fit has been shifted by the apparatus's ion flight constant of 4.5 μs amu$^{-1/2}$ to account for the shorter flight time of the $m/e = 33$ ions through the quadrupole region. The $P(E_T)$ used to fit the $m/e = 33$ data thus characterized the C−Br bond fission events that produced stable radicals.

C. Computational Methods. The geometries and single point energies of 2-bromoethanol-d_4 and the stationary points on the potential energy surface of the OH + C_2D_4 reaction were calculated at the G4//B3LYP level of theory, using the GAUSSIAN09, version A.02, electronic structure package.[48] The geometries were optimized until they converged to a root-mean-square force and a root-mean-square displacement of 1×10^{-5} and 4×10^{-5} (in atomic mass units), respectively. The 6-311++G(3df,2p) basis set was utilized, with a spin-restricted wave function for the closed-shell systems and a spin-unrestricted wave function for the open-shell systems. The optimized geometries for the hydrogenated analogues calculated by Senosiain et al.[23] were used as the initial guesses for the geometries of the deuterated molecules. Single-point energies were zero-point corrected at 0 K. The B3LYP/6-311++G(3df,2p) vibrational frequencies were scaled by 0.9854.[49] Force constants and normalized displacement vectors for the normal modes of vibration of the parent molecule were calculated using the same basis set. In several instances on the PES, the transition state could not be optimized using the B3LYP method, likely due to the flat nature of the potential energy surface in these regions. This problem was also noted in the calculation of the OH + C_2H_4[23] and the OH + C_3H_6[50] PES's. For these cases, we assume that there is essentially no barrier beyond the endoergicity.

III. RESULTS

In this section, we present the velocity map imaging and scattering data for the photodissociation of 2-bromoethanol-d_4. We begin with a discussion of the electronic structure calculations of the parent molecule and potential energy surface for the OH + C_2D_4 reaction. Section IIIB details the center-of-mass translational energy distributions obtained from the detection of bromine atoms in both apparatuses, as well as the anisotropy parameters derived for the primary dissociation. Section IIIC describes the detection of stable CD_2CD_2OH radicals. In section IIID, we utilize energy conservation to obtain a distribution of internal energies of the radicals, and in section IIIE, we use a modified impulsive model to determine a distribution of vibrational energy of the radicals, validating our model by using it to accurately predict the measured translational energy distribution of stable radicals.

A. Electronic Structure Calculations. It has been previously determined that 2-bromoethanol has five stable conformers.[51,52] Our calculations characterized the five analogous stable conformers of 2-bromoethanol-1,1,2,2-d_4. The conformers, denoted Tt, Tg, Gt, Gg, and Gg′, are categorized by two terms. The first describes the dihedral angle between the Br and OH group as either T (trans) or G (gauche). The second term describes the dihedral angle of the hydrogen in the OH group and the rest of the moiety as either t (trans) or g (gauche). There are two conformers with a gauche C−C−O−H bond, denoted Gg and Gg′. The zero-point level of the Gg conformer is slightly lower in energy than that of the trans conformers, due to the energetically favorable interaction between the hydroxyl H and the bromine. The single-point energies were calculated at 0 K and at 353.15 K (the nozzle temperature) and the relative populations of the five conformers are calculated assuming a thermal distribution at the nozzle temperature, accounting for the degeneracy of the gauche conformers. These values are shown in Table 1. If no isomerization is occurring on the excited state, seventy percent of the parent molecules are expected to dissociate from a G-conformer, leading to a highly rotationally excited radical. This will be discussed in further detail in section IIIE.

The CD_2CD_2OH radical has several stable conformers. However, upon dissociation of the C−Br bond, the radical is formed with significant internal energy, so it may easily interconvert between these conformers. Thus we calculate bond energies relative to the lowest energy conformer of the radical. The bond dissociation energies for C−Br bond fission, shown in Table 1, were calculated by subtracting the sum of the zero-point corrected G4 energies of the lowest energy CD_2CD_2OH conformer and $Br(^2P_{3/2})$ from the zero-point corrected G4 energy of each parent molecule conformer.

The calculated stationary points on the potential energy surface of the OH + C_2D_4 reaction are shown in Figure 1 along with the $P(E_{vib})$ determined experimentally as described in section IIIE. The zero-point energies shown relative to the CD_2CD_2OH radical are reported in kcal/mol. When multiple stable conformers are calculated, the energy of the lowest-energy

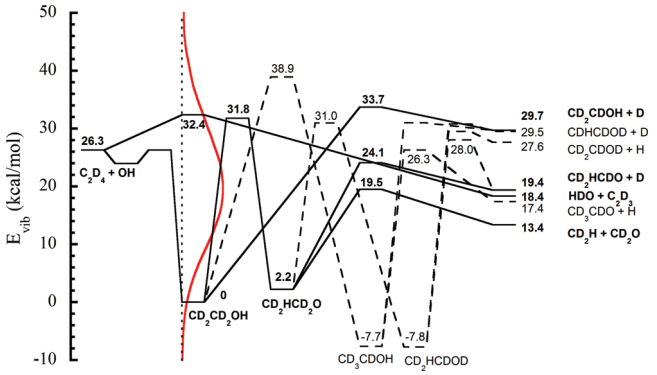

Figure 1. Stationary points on the potential energy surface of the OH + C_2D_4 reaction, calculated at the G4//B3LYP/6-311++G(3df,2p) level of theory. The pathways from the CD_2CD_2OH intermediate shown in black solid line were calculated in ref 33 at the B3LYP/6-311+G(d,p); the additional pathways calculated in this work are shown in dashed line. The $P(E_{vib})$ of CD_2CD_2OH radicals, determined in section IIIE, is shown in red. The energies are shown in kcal/mol, relative to the zero-point energy of the CD_2CD_2OH radical intermediate.

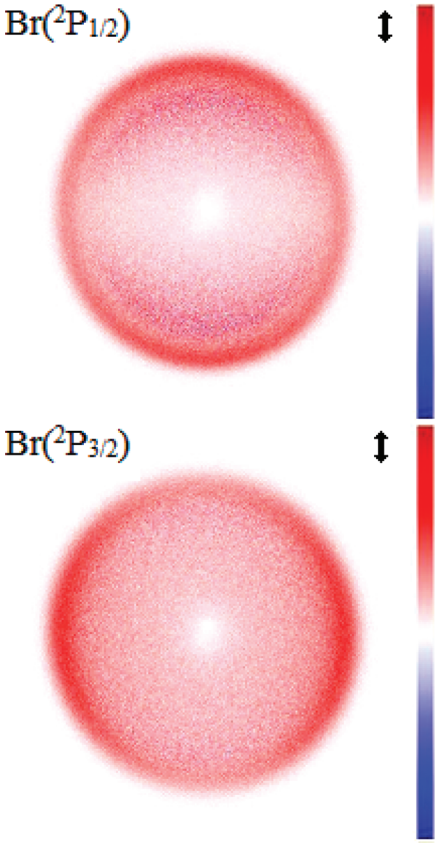

Figure 2. Background-subtracted ion images obtained on the velocity map imaging apparatus. The upper frame shows $Br(^2P_{1/2})$ atoms and the lower frame shows $Br(^2P_{3/2})$ atoms. In both frames the arrow indicates the direction of the laser polarization. Each figure measures 840 × 840 pixels. The ion image of $Br(^2P_{1/2})$ appears to have a faint inner ring. These highly positive (red) and negative (blue) values in this inner ring are noise resulting from subtracting a large photoionization laser background signal in this region.

conformer is reported. In most cases, the energy of the deuterated molecules varies from the hydrogenated analogue by no more than a kcal/mol. Reisler and co-workers[33] calculated the stationary points of several of the deuterated pathways, shown in Figure 1 in black solid line, at the B3LYP/6-311++G(d,p) level of theory. While our calculated G4 endoergicities of the C_2D_4 + OH asymptote and the barrier to isomerize from CD_2CD_2OH to CD_2HCD_2O were similar to the prior B3LYP predictions, the three B3LYP barriers reported in ref 33 to form CD_2CDOH + D, CD_2HCDO + D and CD_2H + CD_2O were substantially higher (by 1.2−2.5 kcal/mol) than our G4 barriers in Figure 1. In addition to these pathways, we also calculated the energies of the product pathways accessed by the α-hydroxyethyl radical (CD_2HCDOD or CD_3CDOH). These pathways are shown in black dashed line in Figure 1. We explored those pathways to predict the likelihood of observing H atom products in addition to D atom products. The results in Figure 1 suggest that the H atom product channels would not be important, because they require surmounting high energy isomerization transition states when lower energy bond fission transition states are available. This conclusion is in agreement with the assignment in ref 33 of the H atom signal to impurities.

The most significant difference between the deuterated PES and the undeuterated PES[23] is the presence of these two isotopic variants of α-hydroxyethyl (CD_3CDOH, which is the product of the isomerization from CD_2CD_2OH, and CD_2HCDOD, which is the product of the isomerization of the partially deuterated ethoxy radical, CD_2HCD_2O). Additionally, there are three isotopic variants of the ethenol + H product channel. The four cases in which the TS could not be optimized with B3LYP were the transition state between CD_2CD_2OH and $[C_2D_4]\cdots OH$, and the three transition states leading from the two α-hydroxyethyl isotopes to ethenol + H. The geometries of the local minima and transition states on the PES and the five parent conformers are reported in the Supporting Information.

B. Translational Energy Distributions Imparted in C−Br Bond Photofission. Figure 2 shows ion images of $Br(^2P_{1/2})$ and $Br(^2P_{3/2})$ atoms obtained on the imaging apparatus in the upper and lower panels respectively. The arrow indicates the direction of the photolysis laser polarization. Both images display a clear anisotropy, which originates from the fact that a molecule is more likely to absorb a photon when the electric vector is aligned with the electronic transition moment vector. The $Br(^2P_{1/2})$ image displays a top-bottom anisotropy, indicating the transition moment vector lies parallel to the C−Br bond, while the $Br(^2P_{3/2})$ image displays an angular distribution with a negative anisotropy parameter, implying that the transition moment vector lies perpendicular to the C−Br bond. The exact anisotropy parameters were obtained by fitting the angular distributions derived from the detection of $Br(^2P_{1/2})$ and $Br(^2P_{3/2})$ to $1 + \beta P_2(\cos\theta)$ and $1 + \beta_2 P_2(\cos\theta) + \beta_4 P_4(\cos\theta)$ respectively, where P_2 and P_4 are second- and fourth-order Legendre polynomials, θ is the angle between the electric vector of the photolysis laser and the radical's recoil velocity vector, and β is the anisotropy parameter.[41] In this case, β_4 was nearly zero, and so β_2 can be treated as the angular anisotropy parameter β. The anisotropy parameter β ranges from −1 to 2, where $\beta = -1$ corresponds to a strongly perpendicular transition and $\beta = 2$ corresponds to a strongly parallel transition. β and β_2 show a significant velocity dependence, with both values becoming more parallel at higher velocities. The $\beta(v)$ spectra are shown in the Supporting Information, and weighted-average values are displayed in Table 2. The values listed are similar to those reported for 2-bromoethanol

dx.doi.org/10.1021/jp2059694 |J. Phys. Chem. A 2011, 115, 14559–14569

Table 2. Weighted-Average Anisotropy Parameters for the Angular Distributions of the Photodissociation Channels Leading to $Br(^2P_{1/2})$ + CD_2CD_2OH and $Br(^2P_{3/2})$ + CD_2CD_2OH

spin−orbit state	anisotropy parameter
$Br(^2P_{1/2})$	$\beta = 0.47$
$Br(^2P_{3/2})$	$\beta_2 = -0.27$
	$\beta_4 = 0.05$

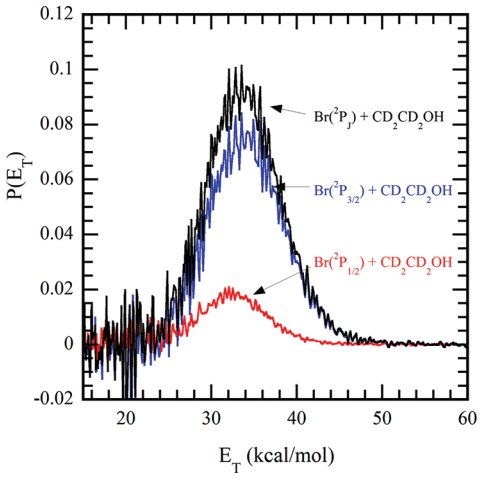

Figure 3. Center-of-mass recoil translational energy distribution of Br + CD_2CD_2OH following the photodissociation of 2-bromoethanol-d_4 at 193 nm. The distributions, obtained on the imaging apparatus by state-selectively detecting the ground and excited spin−orbit states of Br, are weighted by the spin−orbit branching ratio and summed to yield the total $P(E_T)$ shown in black.

photodissociation,[32] confirming that $Br(^2P_{1/2})$ is produced via a transition to the $^3Q_0$ excited state and that $Br(^2P_{3/2})$ is produced via a transition to the $^1Q_1$ or the $^3Q_1$ excited states.[53]

Translational energy distributions, shown in Figure 3, were separately obtained for dissociation events resulting in $Br(^2P_{1/2})$ + CD_2CD_2OH radicals and $Br(^2P_{3/2})$ + CD_2CD_2OH radicals via the state-selective detection of Br. The $P(E_T)$ derived from the velocity distribution of $Br(^2P_{3/2})$ atoms peaks at 35 kcal/mol, while the $P(E_T)$ derived from the velocity distribution of $Br(^2P_{1/2})$ atoms peak at 32 kcal/mol. The two distributions are normalized and weighted by the spin−orbit branching ratio,

$$\frac{N[Br(^2P_{1/2})]}{N[Br(^2P_{3/2})]} = k\frac{S[Br(^2P_{1/2})]}{S[Br(^2P_{3/2})]} \quad (1)$$

which corrects for the relative detection efficiencies of the spin−orbit states of Br. Here, $S[Br(^2P_{1/2})]/S[Br(^2P_{3/2})]$ is the ratio of integrated signal intensity of the spin−orbit states, determined by accumulating bromine signal while scanning over the Doppler profile of each spin−orbit state. It was calculated as 0.756 ± 0.199 after 15 trials. The REMPI line strength k was determined for bromine to be 0.32 ± 0.02.[32] The resulting branching ratio, $N[Br(^2P_{1/2})]/N[Br(^2P_{3/2})]$, is 0.242 ± 0.065. The weighted $P(E_T)$s are added together to yield the total $P(E_T)$ of all dissociation events, shown in black in Figure 3. The $P(E_T)$ peaks near 34 kcal/mol and has an average value of $\langle E_T \rangle$ = 33.6 kcal/mol.

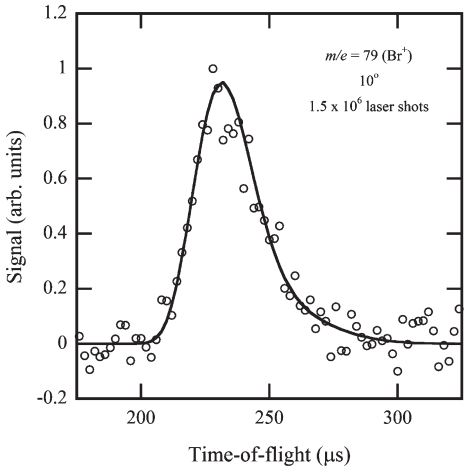

Figure 4. Total time-of-flight spectrum of fragments with a mass-to-charge ratio of 79 following the dissociation of 2-bromoethanol-d_4, detected on the crossed laser-molecular beam scattering apparatus with 200 eV electron bombardment ionization. The data are shown in open circles, and the black line represents the forward convolution fit to the data from the $P(E_T)$ shown in Figure 5.

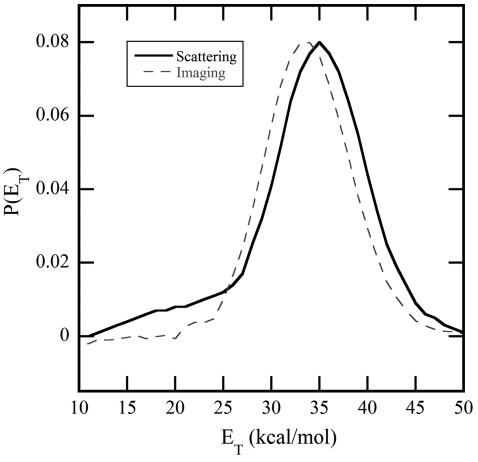

Figure 5. Center-of-mass recoil translational energy distribution, $P(E_T)$, of the photodissociation of 2-bromoethanol-d_4. It was derived by a forward-convolution fit to the $m/e = 79$ (Br^+) scattering apparatus data shown in Figure 4. The smoothed $P(E_T)$ obtained on the imaging apparatus from Figure 3 is shown in gray dashed line for comparison.

Figure 4 shows the time-of-flight spectrum of fragments with $m/e = 79$ (Br^+) obtained in the scattering apparatus. The data are shown in open circles, and the solid black line shows the forward convolution fit. The $P(E_T)$ used to fit these data is shown in solid line in Figure 5 with the smoothed $P(E_T)$ obtained on the imaging apparatus shown in gray dashed line for comparison. It peaks at 35 kcal/mol, with an average $\langle E_T \rangle$ of 34.0 kcal/mol. The maximum value of the $P(E_T)$s from the scattering apparatus and the imaging apparatus agree within 1 kcal/mol, which is within the calibration error for each apparatus.[54] Any small inconsistencies between the two $P(E_T)$s may result from the different expansion conditions of the molecular beam.

In an upcoming manuscript, we consider two additional primary dissociation channels of 2-bromoethanol-d_4, HBr and DBr elimination.[55] These channels were detected at a mass to

dx.doi.org/10.1021/jp2059694 |J. Phys. Chem. A 2011, 115, 14559–14569

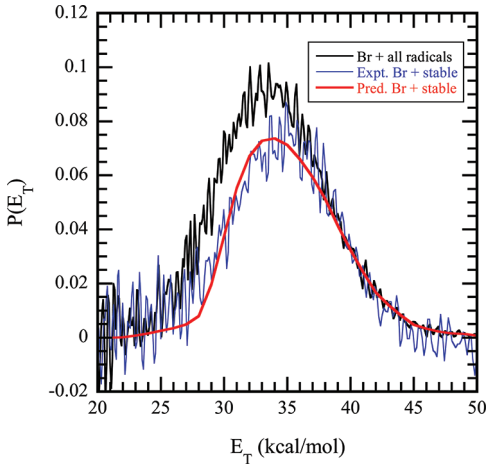

Figure 6. Distribution of recoil translational energies imparted in all C−Br photofission events, shown in black, and of just the photofission events that result in stable CD_2CD_2OH radicals, shown in blue. The two distributions, obtained on the imaging apparatus, were each normalized and scaled such that the fast edges match. The predicted $P(E_T)$ of Br + stable radicals is shown in red, calculated via a modified impulsive model in section IIIE.

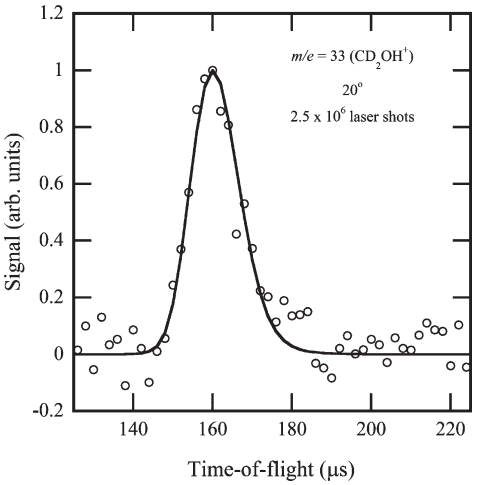

Figure 7. Total time-of-flight spectrum of fragments detected at a mass-to-charge ratio of 33, attributed to CD_2OH^+ ions formed in the dissociative ionization of stable CD_2CD_2OH radicals. The data, obtained on the scattering apparatus, are shown in open circles, and the black line represents the forward convolution fit to the data from the $P(E_T)$ shown in Figure 8.

charge ratio of 82 and 83, respectively, using tunable VUV photoionization and a crossed-laser molecular beam apparatus. The resulting $P(E_T)$s show that the DBr elimination channel imparts less than half the amount of kinetic energy to the resulting fragments than the HBr channel. We consider the possibility that some Br^+ signal is in fact from the dissociative ionization of HBr and DBr. However, we experimentally determined a branching ratio for the C−Br bond fission channel to both the HBr and DBr elimination channels as 168:1 for the HBr channel and 236:1 for the DBr channel. Thus, it is unlikely that a significant portion of the Br^+ signal comes from dissociative ionization.

C. Translational Energy Distributions of Stable CD_2CD_2OH Radicals. Upon photodissociation, Br atoms and CD_2CD_2OH radicals are formed with a range of energies. Br atoms cannot dissociate or isomerize to other products, so the $P(E_T)$ derived from the detection of Br is an effective measurement of all dissociation events. But with sufficient internal energy, CD_2CD_2OH radicals may dissociate to products on a faster time scale than the detection scheme. Thus, the $P(E_T)$ derived from the detection of CD_2CD_2OH radicals is a measurement of the dissociation events that result in radicals that are stable to further dissociation. The comparison of the two $P(E_T)$s provides a measure of the threshold energy at which the radicals can surmount the barrier to dissociation.

The dissociations that result in Br + stable radicals are detected in the imaging apparatus by setting the negative voltage gate to coincide with the arrival of ions with a mass-to-charge ratio of 49 ($CD_2CD_2OH^+$). The resulting ion image is extracted and integrated to yield a velocity distribution of CD_2CD_2OH fragments. Reproducible underlying background signal was apparent in the velocity distribution at nonphysical velocities. This background was attributed to the photoionization laser beam hitting the ion optics assembly and was fit to a Gaussian curve and subtracted out. The raw data and Gaussian curve used are shown in the Supporting Information. Conservation of momentum is used to derive a $P(E_T)$ from the background-subtracted velocity distribution using 80 as the mass of the bromine, to reflect the nearly 50/50 natural isotopic ratio between ^{79}Br and ^{81}Br. Figure 6 shows the $P(E_T)$ of Br + stable CD_2CD_2OH radicals in blue with the $P(E_T)$ of Br + all CD_2CD_2OH radicals shown in black for comparison. The two distributions match closely at high E_Ts, because radicals that have been formed with higher recoil translational energy have significantly less internal energy and are thus stable to further dissociation. Radicals formed in low E_T C−Br fission events, on the other hand, have much more energy available in internal degrees of freedom and therefore a significant fraction have sufficient energy to dissociate and are not detected. The threshold translational energy at which the radicals begin to dissociate is given by the energy at which the two $P(E_T)$s begin to diverge, 39.4 kcal/mol. However, there is a significant portion of stable radicals formed with translational energies below this threshold, due to the creation of rotationally metastable radicals. This will be discussed in further detail in section IIID. A predicted $P(E_T)$ for Br + stable radicals, calculated in section IIIE, is shown in red.

Figure 7 shows the TOF spectrum of m/e = 33 fragments obtained in the scattering apparatus. This signal is attributed to CD_2OH^+, which results from the dissociative ionization of stable CD_2CD_2OH radicals. The data are shown in open circles, and the forward convolution fit is shown as a solid line. No signal was detected above the baseline at m/e = 49 ($CD_2CD_2OH^+$), even after 1.5 × 10^6 laser shots. This is to be expected, as the appearance energy of m/e = 33 (CD_2OH^+) from stable CD_2CD_2OH radicals is 12.02 eV. This appearance energy was calculated as the difference between the zero-point corrected energies of the CD_2CD_2OH radical and the sum of the neutral CD_2 fragment and the CD_2OH^+ ion, calculated at the G4//B3LYP/6-311++G(3df,2p) level of theory. Electron bombardment at 200 eV provides more than enough energy to dissociatively ionize stable radicals into smaller ion fragments. The m/e = 33 signal thus represents CD_2CD_2OH radicals that are stable enough to survive until reaching the ionizer but then undergo dissociation upon electron bombardment ionization. The $P(E_T)$ used to fit the m/e = 33 data, shown in Figure 8, is the same as the

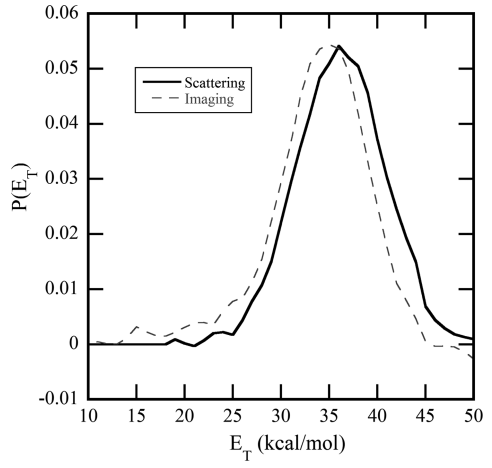

Figure 8. Center-of-mass recoil translational energy distribution of the photodissociation of 2-bromoethanol-d_4 that resulted in stable CD_2CD_2OH radicals. This distribution was obtained by a forward-convolution fit to the $m/e = 33$ (CD_2OH^+) data shown in Figure 7. The smoothed $P(E_T)$ obtained on the imaging apparatus from Figure 6 is shown in gray dashed line for comparison.

one that would be used to fit any stable $m/e = 49$ data. It has an average value of $\langle E_T \rangle = 36.2$ kcal/mol and peaks at $E_T = 36$ kcal/mol. The smoothed $P(E_T)$ obtained on the imaging apparatus at $m/e = 49$ is shown in gray dashed line for comparison. The major portions of the two $P(E_T)$s match within 1 kcal/mol.

D. Derivation of the Internal Energy Distribution of CD_2CD_2OH Radicals. As further studies of the product channels of the OH + C_2D_4 reaction depend on the internal energy of the CD_2CD_2OH radicals, eq 2 is used to derive an internal energy distribution for the nascent radicals from the measured $P(E_T)$ of all C−Br fission events. Conservation of energy requires that the sum of the energy of the photon and the energy of the parent molecule prior to dissociation must be equal to the energy partitioned into the product fragments. Some of this energy is consumed in breaking the C−Br bond, and the remaining energy is distributed among recoil translational energy in the center-of-mass reference frame, E_T, and internal energy of the fragments, $E_{int,Br} + E_{int,radicals}$.

$$E_{photon} + E_{int,parent} = D_0(C\text{-}Br) + E_T + E_{int,Br} + E_{int,radicals} \quad (2)$$

Here, E_{photon} is 147.8 kcal/mol, the energy of the 193.3 nm photon used to break the C−Br bond. The supersonic expansion of the molecular beam effectively cools the rotational degrees of freedom of the parent molecule, so $E_{int,parent}$ consists of the vibrational energy of the parent, calculated by a direct count of eigenstates. The average values of $E_{int,parent}$ for each conformer of 2-bromoethanol-d_4 are approximately 2.5 kcal/mol. D_0 is calculated at the G4//B3LYP/6-311++G(3df,2p) level of theory, as described in section IIIA and the values for each conformer are listed in Table 1. As D_0 is defined here as the difference between the zero-point energies of each of the 2-bromoethanol-d_4 conformers and the lowest energy CD_2CD_2OH conformer, the zero of internal energy calculated in eq 2 is set as the zero-point energy of the CD_2CD_2OH radicals. The range of translational energies, E_T is experimentally determined, as described in section IIIB, and $E_{int,Br}$ is either 0 or 10.54 kcal/mol, depending on which spin−orbit state of bromine is detected. A range of $E_{int,radicals}$ is calculated using these values.

We calculate an approximate lower bound to the range of internal energies accessible to the CD_2CD_2OH radicals. The radicals formed in conjunction with $Br(^2P_{1/2})$ and with the maximum amount of translational energy have about 20 kcal/mol of internal energy. The majority of the radicals have significantly more than 20 kcal/mol of internal energy; some have as much as 60 kcal/mol. The lowest calculated energy barrier for the dissociation of CD_2CD_2OH is the pathway that leads to OH + C_2D_4 and it was calculated to lie 26.3 kcal/mol above the zero-point level of the radical. Therefore, nearly all the radicals are calculated to have internal energy higher than this barrier height. However, the large number of stable radicals that were nevertheless detected, coupled with our previous work[32] which detailed the large amount of rotational energy partitioning that occurs in the dissociation of the analogous 2-bromoethanol, indicate that these internally excited CD_2CD_2OH radicals are similarly stabilized by partitioning internal energy into rotational energy, rather than vibrational energy.

Absorption of a 193 nm photon by the 2-bromoethanol-d_4 molecule excites a transition nominally assigned to promoting an electron from a nonbonding orbital of the bromine to a σ^* antibonding orbital of the C−Br bond, as discussed in ref 56 and references within.[56] The potential energy surface of the excited state accessed by an $n \rightarrow \sigma^*$ absorption band, such as that for the 260 nm absorption band of CH_3I, has been shown to be quite steep in the Franck−Condon region,[57,58] so the reaction should occur in less than a picosecond. This is experimentally confirmed by the marked anisotropy of the angular distributions. The rapid dissociation of the C−Br bond thus generates an impulsive kick to the radical fragment. The resulting force on the radical is positioned far away from the center of mass of the radical, imparting a large amount of rotational energy to the radical. Conservation of angular momentum dictates that little of this energy is available to surmount the energetic barriers of the dissociation pathways. In their study of the photodissociation of 2-bromoethanol, Hintsa et al.[31] noted that an impulsive dissociation of the gauche conformer with an E_T of 33 kcal/mol (the median value) and with an impact parameter of $b = 1.36$ Å would partition 38 kcal/mol to rotation, but that such a dissociation would violate conservation of energy at higher E_Ts. This lead them to suggest that the C−C−Br angle widened during dissociation, a widening that also might result in their observed photofragment angular distribution being isotropic. However, later experiments by Ratliff et al[32] separately resolved the angular distributions of the $Br(^2P_{1/2})$ and $Br(^2P_{3/2})$ cofragments and both are strongly anisotropic, so the isotropic angular distribution measured by Hintsa et al. is simply a weighted average of those two angular distributions. Ratliff et al.[32] developed a modified impulsive model, described in the next section, accounting for zero-point motion in the C−C−Br bend and the thermal distribution of internal energy in the photolytic precursor that correctly modeled the distribution of stable radicals due to partitioning of energy to rotation, if one assumed that many of the 2-bromoethanol molecules isomerized to a trans geometry on the excited state surface prior to the impulsive dissociation. We now use this model to characterize the analogous partitioning to the CD_2CD_2OH radical.

E. Modeling Rotational Energy Partitioning to the CD_2CD_2-OH Radicals. The model described in this section is based on an impulsive model,[59−62] which assumes that the impulsive force on

the repulsive excited state of 2-bromoethanol-d_4 acts in the Franck–Condon region. Unlike classical rigid radical impulsive models, which assume little to none of the energy imparted to the fragments during the dissociation is distributed among the vibrational degrees of freedom, our model uses an experimental distribution of kinetic energies rather than predicting E_T as part of the model. This modeled rotational energy, derived from the measured $P(E_T)$ using conservation of angular momentum, is then subtracted from the calculated distribution of internal energy to determine the vibrational energy imparted to the nascent radicals.

The model has been described in greater detail elsewhere.[32,63] Briefly, conservation of angular momentum requires that the classical orbital angular momentum of the fragments be equal in magnitude but opposite in direction to the rotational angular momentum of the radical. The angular momentum of the photon is neglected here. Substitution of the definitions of rotational and translational energy yields

$$E_{rot} = \frac{\mu b^2}{I} E_T \quad (3)$$

where μ is the reduced mass of the Br + radical system, b is the impact parameter in the C–Br bond fission, and I is the moment of inertia of the CD_2CD_2OH radical fragment about an axis of rotation perpendicular to the plane defined by the center of mass of the radical and the C–Br bond. The $\mu b^2/I$ factor is calculated by a series of vector calculations,[54] given the Cartesian coordinates of the atoms of the parent molecule at equilibrium geometry. The model assumes that the geometry of the CD_2CD_2OH moiety of the 2-bromoethanol-d_4 molecule is preserved upon dissociation.

One key factor included in this model is accounting for the fact that in the low lying vibrational states of the parent molecule, a range of impact parameters and moments of inertia is accessed as the molecule vibrates. The likelihood of the molecule dissociating with a certain $\mu b^2/I$ factor is given by the square of the harmonic wave function at the displacement from equilibrium that yielded that geometry. The majority of the normal modes of vibration of the parent molecule involve only hydrogen or deuterium motion, which makes little difference to the impact parameter. Taking into consideration only the normal vibrational mode that results in the widest range of $\mu b^2/I$ factors, a distribution of rotational energies can be calculated for a given E_T using eq 3. The relevant normal modes used for each of the conformers of 2-bromoethanol-d_4 are ν_3 = 201.37 cm^{-1} for Tt, ν_2 = 194.99 cm^{-1} for Tg, ν_{14} = 1109.61 cm^{-1} for Gt, ν_{13} = 1068.05 cm^{-1}, and ν_{13} = 1068.31 cm^{-1}. Using the relation $E_{int} = E_{vib} + E_{rot}$ and substituting eq 3 into eq 2 yields eq 4.

$$E_{vib} = E_{photon} + E_{int,parent} - D_0(C\text{-}Br) - E_{int,Br} - \left(1 + \frac{\mu b^2}{I}\right) E_T \quad (4)$$

E_{vib} is solved for using the values defined in section IIIC. Rather than use the average value for $E_{int,parent}$, however, a direct count of states yields a distribution of internal energies of the parent molecule, $P(E_{int,parent})$. A complete distribution of vibrational energies partitioned to the radicals, $P(E_{vib})$, is obtained by convoluting the experimental $P(E_T)$ of all radicals over the distribution of $\mu b^2/I$ factors and over the $P(E_{int,parent})$. A separate $P(E_{vib})$ is calculated for each of the stable conformers of 2-bromoethanol-d_4, using the appropriate values for D_0 and $P(E_{int,parent})$. The five distributions are scaled according to the thermal population percentages listed in Table 1 and summed to yield the resulting total $P(E_{vib})$, shown in Figure 1 overlaid on the potential energy surface of the OH + C_2D_4 reaction.

The calculated $P(E_{vib})$ spans energies above and below the theoretically predicted 26.3 kcal/mol barrier height to the OH + C_2D_4 dissociation pathway. In an effort to characterize the accuracy of our model, we apply a vibrational energy cutoff of 26.3 kcal/mol to the calculated $P(E_{vib})$ and assume that all nascent radicals formed with vibrational energy above this cutoff will not be detected because they rapidly undergo secondary dissociation. For every E_T in the $P(E_T)$ of all dissociation events, a distribution of vibrational energies is calculated from eq 4, and the fraction of events that leave the CD_2CD_2OH with low enough E_{vib} to remain stable to further dissociation is calculated by integrating the $P(E_{vib})$ up to the vibrational energy threshold. In this way, we obtain a predicted $P(E_T)$ of Br + stable radicals.

The three G-conformers of 2-bromoethanol-d_4, Gt, Gg, and Gg′, have a much larger impact parameter than the two T-conformers, and thus, the dissociation of the C–Br bond in these molecules imparts a larger amount of energy into rotation, stabilizing those radicals. A predicted $P(E_T)$ of Br + stable radicals is obtained for each of the five conformers and weighted according to their relative thermal populations at the nozzle temperature. The total predicted spectrum is the sum of these predictions and is shown in red in Figure 6. The close match between the predicted spectrum and the experimental spectrum affirms, within 2 kcal/mol, the accuracy of our model and the theoretically calculated barrier height for the dissociation of the radical to OH + C_2D_4.

IV. DISCUSSION

In this study, we photodissociated a precursor, 2-bromoethanol-d_4, to yield momentum-matched bromine atoms and CD_2CD_2OH radical fragments. Using a velocity map imaging apparatus and a crossed laser-molecular beam scattering apparatus, we obtained translational energy distributions for all dissociation events, and for just those events that result in radicals that are stable to further dissociation on the time scale of the measurement. Using conservation of energy and a model for approximating rotational energy partitioning, we determined a distribution of vibrational energies of the nascent CD_2CD_2OH radicals. This distribution, shown in Figure 1, peaks at 19.5 kcal/mol, with 30.7% of the radicals having a vibrational energy larger than the 26.3 kcal/mol threshold needed to access the OH + C_2D_4 product channel, and 16.6% having vibrational energy higher than the 31.8 kcal/mol needed to access the isomerization pathway to CD_2HCD_2O.

The study of this partially deuterated system provides an opportunity to probe the effect of specific deuterium-hydrogen replacements on energy partitioning to the CD_2CD_2OH radicals. There are several key differences between this work and our previous study of the dynamics of the CH_2CH_2OH radical. In the hydrogenated system, the translational energy distributions peak approximately 2 kcal/mol faster than in the deuterated system.[32] Additionally, while the photodissociation of $BrCH_2CH_2OH$ partitions energy into the radical such that 60% of the radicals formed with vibrational energy below that required to dissociate to OH + ethene; the analogous number for the photodissociation of $BrCD_2CD_2OH$ is 76%. This marked increase in the percentage of dissociation events that result in stable radicals is due to the fact that the $P(E_{vib})$ for the CD_2CD_2OH radicals peaks at 19.5 kcal/mol, whereas that for CH_2CH_2OH radicals peaks

7 kcal/mol higher, at 26.5 kcal/mol. In addition, while energy and angular momentum conservation allows the gauche conformer of the $BrCD_2CD_2OH$ molecule to dissociate impulsively from equilibrium geometry, the data on the hydrogenated system indicated the many of the gauche conformers had to isomerize prior to dissociation.

Furthermore, this system allows further testing of our recently proposed rotational model. The model has been assessed in systems in which the excitation of the parent molecule occurs on a potential energy surface that is not repulsive in the Franck−Condon region,[46,63] as well as systems that are repulsive, and thus generate a large recoil kinetic energy in the dissociation.[32] In our studies of the 2-bromoethanol molecule, assuming the excited state molecules dissociated from the ground state thermal distribution of parent conformers resulted in a poor prediction of the experimental stable radical spectrum.[32] To obtain a reasonable prediction, we instead assumed that a certain percentage of the G-conformer parent molecules underwent a conversion to the T-conformer upon excitation. In the deuterated system, however, a good prediction can be attained assuming a thermal distribution of parent molecules at the nozzle temperature. Thus, with no adjustable parameters, the model predicts the measured velocity distribution of stable radicals in the partially deuterated system.

The model relies on the assumption that the torque generating the radical's rotational energy acts in the Franck−Condon region. Though many prior theoretical papers, beginning with studies of triatomic photodissociation by Schinke,[64] have emphasized the importance of considering torques along the entire dissociative trajectory on the excited state potential energy to accurately predict rotational energy partitioning in the photofragments, the present system does not require including such effects to get good agreement with the experimentally measured distribution of stable radicals. Although Hintsa et al. rationalized their isotropic Br angular distribution by concluding that widening of the C−C−Br angle occurs on the potential surface, reducing the torque,[31] later experiments showed the isotropic distribution results from the weighed sum of the highly anisotropic $Br(^2P_{1/2})$ and $Br(^2P_{3/2})$ distributions.[32] In analogy with the excited states of methyl bromide,[65] we expect that the excited states of 2-bromoethanol accessed at 193 nm are steeply repulsive in the C−Br bond in the Franck−Condon region, making the present model a useful one.

We note one simplification in the implementation of the current model. We have assumed that 100% of radicals with vibrational energy above the barrier will dissociate and 0% of those below the barrier will dissociate. This assumption ignores the possibility of tunneling, as well as the possibility of unstable radicals remaining stable during the detection time scale. Though including these effects is important, due to limits in resolution and calibration error, the present experimental data are not sensitive to these small differences. Our results from the two apparatuses with detection time scales of 40 ns (imaging) and >100 μs (scattering) result in similar spectra within these limitations. Plots in the Supporting Information show that changes in the vibrational threshold of up to 2 kcal/mol in either direction do not have a dramatic effect on the shape of the predicted stable radical spectrum.

The calculation of an accurate vibrational energy distribution of CD_2CD_2OH radicals is key to probing the subsequent dissociation channels of the radical as a function of its energy. In our upcoming study,[55] we detect the products formed by the dissociation of the unstable radicals in an effort to characterize the product branching of the reaction. Comparison to the product branching study of the CH_2CH_2OH radical[35] will offer insight into how the product branching changes as a result of partial deuteration. In particular, indication of a frustrated dissociation to OH + ethene leading instead to a vinyl + H_2O channel was evident in our previous study. This product channel, traditionally assigned to a direct hydrogen abstraction reaction by the hydroxyl radical, was previously thought to be inaccessible to the CH_2CH_2OH radicals. Trajectory calculations by Bowman and co-workers have recently suggested a roaming mechanism for this product channel,[66] so it will be interesting to detect the analogous pathway to C_2D_3 + HDO from the radical intermediate of the OH + C_2D_4 reaction.

■ ASSOCIATED CONTENT

Supporting Information. Optimized geometries of 2-bromoethanol-d_4 and the stationary points on the OH + C_2D_4 PES, frequencies, force constants, rotational constants, and normalized displacement vectors for the 2-bromoethanol-d_4 conformers, velocity dependent anisotropy spectra, the underlying background in the CD_2CD_2OH velocity distribution, and additional predicted $P(E_T)$s for Br + stable radicals. This material is available free of charge via the Internet at http://pubs.acs.org.

■ AUTHOR INFORMATION

Corresponding Authors

*E-mail: L-Butler@uchicago.edu (L.J.B.); dszpunar@roosevelt.edu (D.E.S.).

■ ACKNOWLEDGMENT

This work was supported by the Department of Energy, Basic Energy Sciences, under contract number DE-FG02-92ER14305. We would like to thank Prof. Hanna Reisler for sharing the results of her deuterated 2-hydroxyethyl work.

■ REFERENCES

(1) Vakhtin, A. B.; Murphy, J. E.; Leone, S. R. *J. Phys. Chem. A* **2003**, *107*, 10055.
(2) Bradley, J. N.; Capey, W. D.; Fair, R. W.; Pritchard, D. K. *Int. J. Chem. Kinet.* **1976**, *8*, 549.
(3) Tully, F. P. *Chem. Phys. Lett.* **1983**, *96*, 148.
(4) Tully, F. P. *Chem. Phys. Lett.* **1988**, *143*, 510.
(5) Morris, E. D.; Stedman, D. H.; Niki, H. *J. Am. Chem. Soc.* **1971**, *93*, 3570.
(6) Cool, T. A.; Nakajima, K.; Mostefaoui, T. A.; Qi, F.; McIlroy, A.; Westmoreland, P. R.; Law, M. E.; Poisson, L.; Peterka, D. S.; Ahmed, M. *J. Chem. Phys.* **2003**, *119*, 8356.
(7) Taatjes, C. A.; Hansen, N.; McIlroy, A.; Miller, J. A.; Senosiain, J. P.; Klippenstein, S. J.; Qi, F.; Sheng, L. S.; Zhang, Y. W.; Cool, T. A.; Wang, J.; Westmoreland, P. R.; Law, M. E.; Kasper, T.; Kohse-Hoinghaus, K. *Science* **2005**, *308*, 1887.
(8) Taatjes, C. A.; Hansen, N.; Miller, J. A.; Cool, T. A.; Wang, J.; Westmoreland, P. R.; Law, M. E.; Kasper, T.; Kohse-Hoinghaus, K. *J. Phys. Chem. A* **2006**, *110*, 3254.
(9) Bradley, J. N.; Hack, W.; Hoyerman, K.; Wagner, H. G. *J. Chem. Soc., Faraday Trans. I* **1973**, *69*, 1889.
(10) Smith, I. W. M.; Zellner, R. *J. Chem. Soc., Faraday Trans. II* **1973**, *69*, 1617.
(11) Farquharson, G. K.; Smith, R. H. *Aust. J. Chem.* **1980**, *33*, 1425.

(12) Atkinson, R.; Aschmann, S. M.; Winer, A. M.; Pitts, J. N. *Int. J. Chem. Kinet.* **1982**, *14*, 507.
(13) Atkinson, R.; Aschmann, S. M. *Int. J. Chem. Kinet.* **1984**, *16*, 1175.
(14) Liu, A. D.; Mulac, W. A.; Jonah, C. D. *Int. J. Chem. Kinet.* **1987**, *19*, 25.
(15) Liu, A. D.; Mulac, W. A.; Jonah, C. D. *J. Phys. Chem.* **1988**, *92*, 3828.
(16) Bott, J. F.; Cohen, N. *Int. J. Chem. Kinet.* **1991**, *23*, 1075.
(17) Becker, K. H.; Geiger, H.; Wiesen, P. *Chem. Phys. Lett.* **1991**, *184*, 256.
(18) Kuo, C.-H.; Lee, Y. P. *J. Phys. Chem.* **1991**, *95*, 1253.
(19) Diau, E. W.-G.; Lee, Y. P. *J. Chem. Phys.* **1992**, *96*, 377.
(20) Chuong, B.; Stevens, P. S. *J. Phys. Chem. A* **2000**, *104*, 5230.
(21) Klein, T.; Barnes, I.; Becker, K. H.; Fink, E. H.; Zabel, F. *J. Phys. Chem.* **1984**, *88*, 5020.
(22) Zhu, R. S.; Park, J.; Lin, M. C. *Chem. Phys. Lett.* **2005**, *408*, 25.
(23) Senosiain, J. P.; Klippenstein, S. J.; Miller, J. A. *J. Phys. Chem. A* **2006**, *110*, 6960.
(24) Sosa, C.; Schlegel, H. B. *J. Am. Chem. Soc.* **1987**, *109*, 7007.
(25) Yamada, T.; Bozzelli, J. W.; Lay, T. *J. Phys. Chem. A* **1999**, *103*, 7646.
(26) Hippler, H.; Viskolcz, B. *Phys. Chem. Chem. Phys.* **2000**, *2*, 3591.
(27) Srinivasan, N. K.; Su, M. C.; Michael, J. V. *Phys. Chem. Chem. Phys.* **2007**, *9*, 4155.
(28) Sosa, C.; Schlegel, H. B. *J. Am. Chem. Soc.* **1987**, *109*, 4193.
(29) Ziemann, P. J. *Int. Rev. Phys. Chem.* **2011**, *30*, 161.
(30) Sapers, S. P.; Hess, W. P. *J. Chem. Phys.* **1992**, *97*, 3126.
(31) Hintsa, E. J.; Zhao, X. S.; Lee, Y. T. *J. Chem. Phys.* **1990**, *92*, 2280.
(32) Ratliff, B. J.; Womack, C. C.; Tang, X. N.; Landau, W. M.; Butler, L. J.; Szpunar, D. E. *J. Phys. Chem. A* **2010**, *114*, 4934.
(33) Edwards, L. W.; Ryazanov, M.; Reisler, H.; Klippenstein, S. J. *J. Phys. Chem. A* **2010**, 5453.
(34) Shubert, V. A.; Rednic, M.; Pratt, S. T. *J. Phys. Chem. A* **2009**, *113*, 9057.
(35) Ratliff, B. J.; Alligood, B. W.; Butler, L. J.; Lee, S.-H.; Lin, J. J. M. *J. Phys. Chem. A* **2011**, *115*, 9097.
(36) Parker, D. H.; Eppink, A. T. J. B. *J. Chem. Phys.* **1997**, *107*, 2357.
(37) Eppink, A. T. J. B.; Parker, D. H. *Rev. Sci. Instrum.* **1997**, *68*, 3477.
(38) Miller, D. R. Free Jet Sources. In *Atomic and Molecular Beam Methods*; Scoles, G., Ed.; Oxford University Press: New York, 1988; pp 14−53.
(39) Ruoff, R. S.; Klots, T. D.; Emilsson, T.; Gutowsky, H. S. *J. Chem. Phys.* **1990**, *93*, 3142.
(40) Chang, B. Y.; Hoetzlein, R. C.; Mueller, J. A.; Geiser, J. D.; Houston, P. L. *Rev. Sci. Instrum.* **1998**, *69*, 1665.
(41) Thoman, J. W.; Chandler, D. W.; Parker, D. H.; Janssen, M. H. M. *Laser Chem.* **1988**, *9*, 27.
(42) Heck, A. J. R.; Chandler, D. W. *Annu. Rev. Phys. Chem.* **1995**, *46*, 335.
(43) Dasch, C. J. *Appl. Opt.* **1992**, *31*, 1146.
(44) Dribinski, V.; Ossadtchi, A.; Mandelshtam, V. A.; Reisler, H. *Rev. Sci. Instrum.* **2002**, *73*, 2634.
(45) Alligood, B. W.; FitzPatrick, B. L.; Glassman, E. J.; Butler, L. J.; Lau, K. C. *J. Chem. Phys.* **2009**, *131*, 44305.
(46) Alligood, B. W.; FitzPatrick, B. L.; Szpunar, D. E.; Butler, L. J. *J. Chem. Phys.* **2011**, *134*, 54301.
(47) FitzPatrick, B. L.; Alligood, B. W.; Butler, L. J.; Lee, S.-H.; Lin, J. J. *J. Chem. Phys.* **2010**, *133*, 94306.
(48) Frisch, M. J.; Trucks, G. W.; Schlegel, H. B. et al. *Gaussian 09*, Revision A.02; Gaussian, Inc.: Wallingford, CT, 2009.
(49) Curtiss, L. A.; Redfern, P. C.; Raghavachari, K.; Pople, J. A. *J. Chem. Phys.* **2001**, *114*, 108.
(50) Zador, J.; Jasper, A. W.; Miller, J. A. *Phys. Chem. Chem. Phys.* **2009**, *11*, 11040.
(51) Azrak, R. G.; Wilson, E. B. *J. Chem. Phys.* **1970**, *52*, 5299.
(52) Thomassen, H.; Samdal, S.; Hedberg, K. *J. Phys. Chem.* **1993**, *97*, 4004.
(53) Van Veen, G. N. A.; Baller, T.; De Vries, A. E. *Chem. Phys.* **1985**, *92*, 59.
(54) Szpunar, D. E. Centrifugal Effects in the Dissociation Dynamics of Allyl Iodide and Rotationally Excited Allyl Radicals, Appendix C. *Ph.D. Thesis*; University of Chicago, Chicago IL, 2003.
(55) Womack, C. C.; Ratliff, B. J.; Butler, L. J.; Lee, S.-H.; Lin, J. J. M.; *Manuscript in Preparation*, 2011.
(56) Butler, L. J.; Hintsa, E. J.; Shane, S. F.; Lee, Y. T. *J. Chem. Phys.* **1987**, *86*, 2051.
(57) Krajnovich, D.; Butler, L. J.; Lee, Y. T. *J. Chem. Phys.* **1984**, *81*, 3031.
(58) Khundkar, L. R.; Zewail, A. H. *Chem. Phys. Lett.* **1987**, *142*, 426.
(59) Riley, S. J.; Wilson, K. R. *Faraday Discuss. Chem. Soc.* **1972**, *53*, 132.
(60) Busch, G. E.; Wilson, K. R. *J. Chem. Phys.* **1972**, *56*, 3626.
(61) Holdy, K. E.; Klotz, L. C.; Wilson, K. R. *J. Chem. Phys.* **1970**, *52*, 4588.
(62) North, S. W.; Blank, D. A.; Gezelter, J. D.; Longfellow, C. A.; Lee, Y. T. *J. Chem. Phys.* **1995**, *102*, 4447.
(63) Womack, C. C.; Fang, W. H.; Straus, D. B.; Butler, L. J. *J. Phys. Chem. A* **2010**, *114*, 13005.
(64) Schinke, R. *Photodissociation Dynamics*; Cambridge University Press: Cambridge, 1993; pp 251−255.
(65) Escure, C.; Leininger, T.; Lepetit, B. *J. Chem. Phys.* **2009**, *130*, 244305.
(66) Kamarchik, E.; Koziol, L.; Reisler, H.; Bowman, J. M.; Krylov, A. I. *J. Phys. Chem. Lett.* **2010**, *1*, 3058.